Landau Levels and Magneto-Absorption in InSb†

R. L. Bell and K. T. Rogers*
Varian Associates, Palo Alto, California
(Received 16 June 1966; revised manuscript received 3 August 1966)

Detailed results are presented of machine calculations of the Landau level structure and transition matrix elements for InSb near the center of the Brillouin zone, for magnetic fields in the [100] direction, and under conditions typical of valence-band cyclotron resonance and interband magneto-optical experiments. Effects of inversion asymmetry arising in the zinc-blende structure are included. The theoretical conduction-band combinational resonance spectra of Rashba and Sheka are confirmed and extended to the nonparabolic-band model. The results show good agreement with the recent interband magneto-optical observations by Pidgeon and Brown. Different heavy hole "masses" are predicted for valence-band cyclotron resonance under different experimental conditions. Some of these coincide with reported experimental results. Details of the predicted spin-split zero-field band structure in the (110) plane are given.

I. INTRODUCTION

THEORETICAL band-structure models for the III–V compound semiconductors[1] that crystallize in the zinc-blende structure have been derived from related band structures of Group-IV elements, crystallizing in the diamond lattice, by perturbation methods. The perturbation in question arises with the lifting of the inversion-symmetry degeneracy of the diamond lattice. Thus a zero-order approximation to the Landau level structure of InSb in a magnetic field is provided by that of Ge[2,3] with suitably modified parameters. This approximation has been used, for example, in interpretations of experimental magneto-optical[4] and cyclotron-resonance[5] results in InSb. An effective-mass treatment of the conduction band which includes both magnetic field and inversion-asymmetry effects up to terms of order k^2 has been developed by Rashba and Sheka[6] and applied by them to problems of "combinational resonance" in InSb.[7] An improved treatment of interband effects has recently been given by Pidgeon and Brown,[8] to whose paper we refer for a recent survey of that area.

In this paper we present the results of machine calculations of the Landau levels, and interband and intraband matrix elements near the center of the zone in InSb. In order to minimize the amount of computation involved, a single fixed direction of magnetic field is chosen, namely, parallel to the crystalline (100) axis. The small energy separation of the conduction and valence bands at the center of the zone forces an accurate treatment of these levels. Using a slight modification of the method of Kane,[9] the mutual interactions of these bands are written down to second order in all the perturbations, and the complete matrix which results is diagonalized exactly. At zero field the bands obtained exhibit explicitly the splitting of the spin degeneracy for general points in the zone, due to the inversion asymmetry. At moderate fields, the valence band exhibits the complex behavior anticipated by Dresselhaus.[10]

II. THE HAMILTONIAN

The Hamiltonian of the magnetic-field problem with spin orbit coupling is

$$\mathcal{H}=\frac{1}{2m}\left(\mathbf{p}-\frac{e\mathbf{A}}{c}\right)^2+\frac{\hbar}{4m^2c^2}\left[\nabla V\times\left(\mathbf{p}-\frac{e\mathbf{A}}{c}\right)\right]\cdot\boldsymbol{\sigma}-\frac{e}{2mc}\boldsymbol{\sigma}\cdot\mathbf{H}. \quad (2.1)$$

The field is taken to lie along the z direction, and adopting the Luttinger-Kohn[11] representation, the eigenfunctions may be written[3,12]

$$\Psi_p=\sum_{i,n}\alpha_{\mathrm{in}p}e^{i(k_1x+k_3z)}f_n(y)\phi_i(r). \quad (2.2)$$

The f_n are harmonic-oscillator functions of the transverse coordinate. The ϕ_i are the Bloch band-edge functions $u_{n0}(r)$, and at the center of the zone belong to the five representations (Dresselhaus[10]) Γ_1 through Γ_5 of T_d. Explicit band-edge functions may be constructed from appropriate pairs of the cubic lattice-harmonics,[13] one from each of the ten representations

† Work supported in part by the U. S. Air Force Avionics Laboratory, Wright-Patterson Air Force Base, under Contract AF 33(657)-9192.
* Now at Stanford Research Institute, Menlo Park, California.
[1] For a recent survey review see O. Madelung, *Physics of III-V Compounds* (John Wiley & Sons, Inc., New York, 1964).
[2] G. Dresselhaus, A. F. Kip, and C. Kittel, Phys. Rev. **98**, 368 (1955).
[3] J. M. Luttinger, Phys. Rev. **102**, 1030 (1956).
[4] L. M. Roth, B. Lax, and S. Zwerdling, Phys. Rev. **114**, 90 (1959); E. Burstein, G. S. Picus, R. F. Wallis, and F. Blatt, *ibid.* **113**, 15 (1959); S. Zwerdling, W. H. Kleiner, and J. P. Theriault, in *Proceedings of the International Conference on the Physics of Semiconductors, Exeter, 1962* (The Institute of Physics and The Physical Society, London, 1962), p. 455; J. Appl. Phys. **32**, 2118 (1961); R. L. Bell and K. T. Rogers, Appl. Phys. Letters **5**, 9 (1964).
[5] D. M. S. Bagguley, M. L. A. Robinson, and R. A. Stradling, Phys. Letters **6**, 143 (1963).
[6] E. I. Rashba and V. I. Sheka, Fiz. Tverd. Tela **3**, 1735 (1961) [English transl.: Soviet Phys.—Solid State **3**, 1257 (1961)].
[7] E. I. Rashba and V. I. Sheka, Fiz. Tverd. Tela **3**, 1863 (1961) [English transl.: Soviet Phys.—Solid State **3**, 1357 (1961)].
[8] C. R. Pidgeon and R. N. Brown, Bull. Am. Phys. Soc. **11**, 52 (1966); Phys. Rev. **146**, 575 (1966).
[9] E. O. Kane, J. Phys. Chem. Solids **1**, 249 (1957).
[10] G. Dresselhaus, Phys. Rev. **100**, 580 (1955).
[11] J. M. Luttinger and W. Kohn, Phys. Rev. **97**, 869 (1955).
[12] V. Evtuhov, Phys. Rev. **125**, 1869 (1962).
[13] D. G. Bell, Rev. Mod. Phys. **26**, 311 (1954).

$\left(F+\frac{\hbar^2}{2m}\right)k^2+E_g+\sigma$	0	$2G\{k_y\ k_z\}-iPk_x$	$2G\{k_x\ k_z\}-iPk_y$	$2G\{k_x\ k_y\}-iPk_z$	0	0	0
0	$\left(F+\frac{\hbar^2}{2m}\right)k^2+E_g-\sigma$	0	0	0	$2G\{k_y\ k_z\}-iPk_x$	$2G\{k_x\ k_z\}-iPk_y$	$2G\{k_x\ k_y\}-iPk_z$
$2G\{k_z\ k_y\}+iPk_x$	0	$\left(A+B+\frac{\hbar^2}{2m}\right)k_x^2$ $+\left(C+D+\frac{\hbar^2}{2m}\right)(k_y^2+k_z^2)$ $+E_2+\sigma+H_6k_z+J_6$	$C_1[k_x,k_y]$ $+D_1\{k_x\ k_y\}-iJ_7$	$C_1[k_x,k_z]$ $+D_1\{k_x\ k_z\}-H_7k_x$	iH_6k_y	$-iH_7k^-$	$H_7k_z+J_7$
$2G\{k_x\ k_z\}+iPk_y$	0	$C_1[k_y,k_x]$ $+D_1\{k_y\ k_x\}+iJ_7$	$\left(A+B+\frac{\hbar^2}{2m}\right)k_y^2$ $+\left(C+D+\frac{\hbar^2}{2m}\right)(k_x^2+k_z^2)$ $-H_6k_z+E_2+\sigma+J_6$	$C_1[k_y,k_z]$ $+D_1\{k_y\ k_z\}+H_7k_y$	$-iH_7k^-$	H_6k_x	$iH_7k_z-iJ_7$
$2G\{k_y\ k_x\}+iPk_z$	0	$C_1[k_z,k_x]$ $+D_1\{k_z\ k_x\}-H_7k_x$	$C_1[k_z,k_y]$ $+D_1\{k_z\ k_y\}+H_7k_y$	$\left(A+B+\frac{\hbar^2}{2m}\right)k_z^2$ $+\left(C+D+\frac{\hbar^2}{2m}\right)(k_x^2+k_y^2)$ $+E_2+\sigma+J_6$	$H_7k_z-J_7$	$iH_7k_z+iJ_7$	$-H_6k^+$
0	$2G\{k_z\ k_y\}+iPk_x$	$-iH_6k_y$	iH_7k^+	$H_7k_z-J_7$	$\left(A+B+\frac{\hbar^2}{2m}\right)k_x^2$ $+\left(C+D+\frac{\hbar^2}{2m}\right)(k_y^2+k_z^2)$ $-H_6k_z+E_2-\sigma+J_6$	$C_1[k_x,k_y]$ $+D_1\{k_x\ k_y\}+iJ_7$	$C_1[k_x,k_z]$ $+D_1\{k_x\ k_z\}+H_7k_x$
0	$2G\{k_z\ k_x\}+iPk_y$	iH_7k^+	H_6k_x	$-iH_7k_z-iJ_7$	$C_1[k_y,k_x]$ $+D_1\{k_y\ k_x\}-iJ_7$	$\left(A+B+\frac{\hbar^2}{2m}\right)k_y^2$ $+\left(C+D+\frac{\hbar^2}{2m}\right)(k_x^2+k_z^2)$ $+H_6k_z-\sigma+E_2+J_6$	$C_1[k_y,k_z]$ $+D_1\{k_y\ k_z\}-H_7k_y$
0	$2G\{k_y\ k_x\}+iPk_z$	$H_7k_z+J_7$	$-iH_7k_z+iJ_7$	$-H_6k^-$	$C_1[k_z,k_x]$ $+D_1\{k_z\ k_x\}+H_7k_x$	$C_1[k_z,k_y]$ $+D_1\{k_z\ k_y\}-H_7k_y$	$\left(A+B+\frac{\hbar^2}{2m}\right)k_z^2$ $+\left(C+D+\frac{\hbar^2}{2m}\right)(k_x^2+k_y^2)$ $+E_2-\sigma+J_6$

FIG. 1. 8×8 Hamiltonian matrix.

of the full cubic group. Certain terms of (2.1) are regarded as perturbations on a soluble Hamiltonian. Matrix elements of (2.1) between the bands of direct interest are calculated in zero, first, and second order in the perturbations, and the eigenvalues found by the secular determinant method. To second order the (mk) element of an approximate Hamiltonian matrix is

$$\sum_n{}' \frac{H_{mn}{}^{(1)}H_{nk}{}^{(1)}}{E_m-E_n}+H_{mk}{}^{(1)}+H_{mk}{}^{(2)}. \tag{2.3}$$

As is well known, the operators in (2.3) do not commute in the presence of a magnetic field. Strict adherence to the above scheme, with no artificial symmetrization, leads directly to the antisymmetrical Hamiltonian, first discussed by Luttinger.[3] Using the Landau gauge,

$$\mathbf{A}=(-Hy,\ 0,\ 0) \tag{2.4}$$

Evtuhov[12] has derived the Schrödinger equation in the band-edge functions. In Evtuhov's notation,

$$\sum_i\sum_n \alpha_{in}f_n\left[-\frac{h^2}{2m}\nabla^2\phi_i+V(r)\phi_i\right]+\alpha_{in}f_n\frac{\hbar}{4m^2c^2}[\boldsymbol{\nabla}V\times\mathbf{p}]\cdot\boldsymbol{\sigma}\phi_i+\sum_i\sum_n \alpha_{in}\frac{h^2}{4m^2c^2}[\boldsymbol{\nabla}V\times\mathbf{k}'f_n]\cdot\boldsymbol{\sigma}\phi_i-\alpha_{in}f_n\frac{e}{2mc}\boldsymbol{\sigma}\cdot\mathbf{H}\phi_i$$
$$+\sum_i\sum_n \alpha_{in}\left[\phi_i\frac{h^2}{2m}k'^2f_n-\frac{ih^2}{m}(\mathbf{k}'f_n)\cdot\boldsymbol{\nabla}\phi_i\right]=E\sum_i\sum_n \alpha_{in}f_n\phi_i, \tag{2.5}$$

where $\mathbf{k}'$ is the equivalent wave vector defined by Evtuhov,[12] which reduces to $\mathbf{k}$ in the absence of magnetic field. In the following we omit the prime, since no confusion should result.

As shown by Kane,[9] the term involving $\nabla V\times\mathbf{k}'$ may be absorbed into other linear-k terms which arise in second order. The first three and the last terms of Eq. (2.5) constitute a zero magnetic field Schrödinger

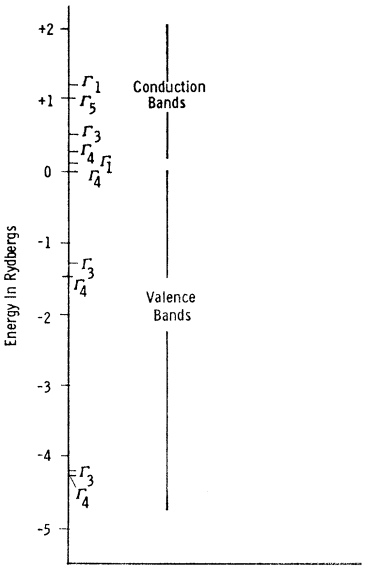

FIG. 2. Approximate energy-level scheme at the center of the zone.

equation including spin-orbit coupling but without the $\mathbf{k}\cdot\mathbf{p}$ perturbation of band theories. The eigenfunctions of the zero-order equation are representations of the double group, which could be taken as a basis for a treatment which regarded the remaining terms of (2.5) as perturbations. In the present case, the algebra is appreciably reduced if the representations of the single group are chosen as a basis, i.e., the zero-order Schrödinger equation is taken to be given by the first two terms together with the last term of (2.5). This may speed up or slow down convergence of the machine diagonalization of the final matrix, but otherwise does not contribute significantly to the accuracy or otherwise of the final results. The basis chosen is thus represented by the eight functions

$$S\uparrow S\downarrow X\uparrow Y\uparrow Z\uparrow X\downarrow Y\downarrow Z\downarrow. \tag{2.6}$$

The S represent the Γ_1-type conduction-band spin-up and -down functions and the X, Y, and Z represent the Γ_4 functions (mainly p type) from which the valence bands derive. The approximate zero-order energies of these states (Kane[9]) are $E_s=E_1$, the measured band gap energy, and $E_p=-\frac{1}{3}\Delta$, where Δ is the observed spin-orbit splitting in the solid. In accordance with (2.3) we write down the first and second-order interactions between the above basis functions for each of the "perturbing" terms of (2.5), i.e., the third (spin-orbit), fifth (Zeeman), sixth (k squared), and seventh ($\mathbf{k}\cdot\mathbf{p}$ perturbation). Second-order matrices are conveniently generated by calculating matrices of these four interactions between the eight basis functions and higher and lower Γ_1 through Γ_5 band edges, and multiplying out the relevant pairs of matrices. The final 8×8 Hamiltonian matrix, to terms in second order, is shown in Fig. 1.

In Fig. 1, the coefficients A through G and the matrix element P are identical with those defined by Kane.[9] E_g is the observed energy gap, and is equal to the energy E_1 defined above, apart from a negligible second-order spin-orbit term due to interaction with Γ_5 levels. The following abbreviations are used:

$$C_1=\tfrac{1}{2}(A+D-C-\tfrac{1}{2}B), \tag{2.7}$$

$$D_1=A+C-D-\tfrac{1}{2}B, \tag{2.8}$$

$$H_6=2(H_2-H_3), \tag{2.9}$$

where

$$H_2=\frac{\hbar^2}{4m^3c^2}\sum_{nl}\frac{\langle X|p_z|\Gamma_4(nl)\rangle\langle\Gamma_4(nl)\uparrow|\nabla V\times\mathbf{p}\cdot\boldsymbol{\sigma}|X\uparrow\rangle}{E_0-E_n}, \tag{2.10}$$

and H_3 is a similar expression with Γ_4 replaced by Γ_5,

$$J_6=2(J_3+J_4), \tag{2.11}$$

$$J_3=\frac{\hbar^2}{8m^4c^4}\sum_{nl}\frac{|\langle Z\uparrow|\nabla V\times\mathbf{p}\cdot\boldsymbol{\sigma}|\Gamma_3(nl)\uparrow\rangle|^2}{E_0-E_n}, \tag{2.12}$$

$$J_4=\frac{\hbar^2}{16m^4c^4}\sum_{nl}\frac{|\langle X\uparrow|\nabla V\times\mathbf{p}\cdot\boldsymbol{\sigma}|\Gamma_4(nl)\uparrow\rangle|^2}{E_0-E_n}, \tag{2.13}$$

$$J_7=J_3-J_4+\tfrac{1}{3}\Delta, \tag{2.14}$$

$$H_7=H_1-H_2-H_3, \tag{2.15}$$

$$H_1=\frac{\hbar^2}{2\sqrt{3}m^3c^2}\sum_{nl}\frac{\langle Y\uparrow|p_y|\Gamma_3(nl)\uparrow\rangle\langle\Gamma_3(nl)\uparrow|\nabla V\times\mathbf{p}\cdot\boldsymbol{\sigma}|Z\uparrow\rangle}{E_0-E_n}$$

$$=-2K_2, \tag{2.16}$$

where K_2 is the coefficient defined by Kane.[9] C_1 is re-

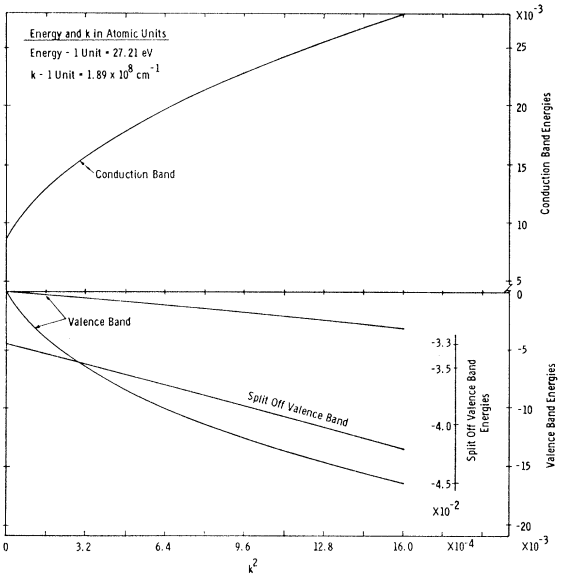

FIG. 3. Energy versus squared wave vector ($\phi=0°$, [100] direction).

lated to Luttinger's[3] antisymmetric constant K; $C_1=\frac{1}{2}\hbar K$. In Fig. 1 we have, further, $\sigma=eH_z/2mc$, $\{k_xk_y\}=\frac{1}{2}(k_xk_y+k_yk_x)$, etc., and $[k_x,k_y]=k_xk_y-k_yk_x$, etc. Finally,

$$-E_2=\tfrac{1}{3}\Delta=i\hbar\langle X\uparrow|\nabla V\times\mathbf{p}\cdot\boldsymbol{\sigma}|Y\uparrow\rangle/4m^2c^2, \quad (2.17)$$

and

$$k^{\pm}=k_x\pm ik_y. \quad (2.18)$$

III. ESTIMATION OF PARAMETERS

In the absence of a complete self-consistent solution of the zero-field band structure, we rely on experiment for estimates of the parameters used above. From the observed conduction-band mass, Kane[9] arrived at a value of 0.44 a.u. for the square of the matrix element P. His estimate of the spin-orbit splitting Δ at the center of the zone, 0.9 eV, appears to be as accurate as any other[1,4,14] and is used here. Bagguley *et al.*[5] deduced other parameters from cyclotron-resonance measurements on p-type InSb. These were: $P^2=0.3$ a.u., $A=0$,

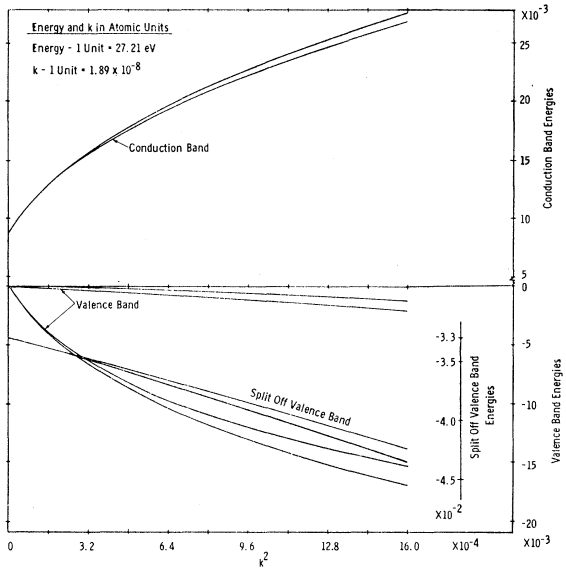

FIG. 4. Energy versus squared wave vector ($\phi=30°$).

$B=-2.4\hbar^2/2m$, $C=-4.7\hbar^2/2m$, and $D=0$. The discrepancy in P^2 appears to be due to the effects of higher bands. The band gap at zero temperature is taken to be 0.237 eV.

In order to estimate the coefficients, we adopt the schematic arrangement of energy levels at the center of the zone shown in Fig. 2. The highest valence band has Γ_4 symmetry (before spin-orbit splitting). The In $4d$ band is known to lie[15] about 1.3 Ry below this, and will be split by the cubic field into levels of Γ_4 and Γ_3 symmetry in the single group. The Sb $4d$ band must lie still lower, at about -4.2 Ry. The lowest conduction band, arising from $5s$ functions, is assigned Γ_1 symmetry. A Γ_4 band lies at about $+0.25$ Ry, as deduced from reflectance measurements.[15] In order to account for cyclotron resonance measurements[5] we tentatively place a Γ_3 level at $+0.5$ Ry. This is not incompatible with the levels of the empty cubic lattice. Γ_1 and Γ_5 levels probably arise at energies of $+1$ Ry or higher. We may first note that the value of the coefficient C is confirmed by the optical measurements. The square of the momentum matrix element in the numerator, for Ge, is about 15 eV,[16] and should be close to this in InSb. The energy difference in the denominator, from the optical gap, is -3.4 eV for InSb, and the ratio is therefore -4.4. This may be compared with a C coefficient estimated from cyclotron resonance of $-4.7\pm10\%$. Assuming a representative value for the square of the matrix element $\langle S|p_x|\Gamma_4\rangle$ of 10 eV, and an energy gap $E_0-E(\Gamma_4)=-3.4$ eV, we have a value for the coefficient F which is the ratio of these, namely, $F=-3.0\hbar^2/2m$. Using the value given above of 15 eV for the square of $\langle\Gamma_4|p_z|X\rangle$ and the same energy gap yields a value for the coefficient G of $-3.6\hbar^2/2m$.

As regards the coefficients H_1, H_2, and H_3, we have increased Kane's estimate of $K_2(=-\frac{1}{2}H_1)$ to take into account the fact that the In $4d$ band is found[15] to be much closer than estimated by Kane,[9] and that interactions with other Γ_3 levels are also present. In combination, these effects may raise H_1 to the order of 10^{-2} a.u. Part of this increase is cancelled by contributions from the Γ_4 levels which complete the fivefold degeneracy of the parent d levels. The Γ_4 contributions are represented above by the coefficient H_2. We have

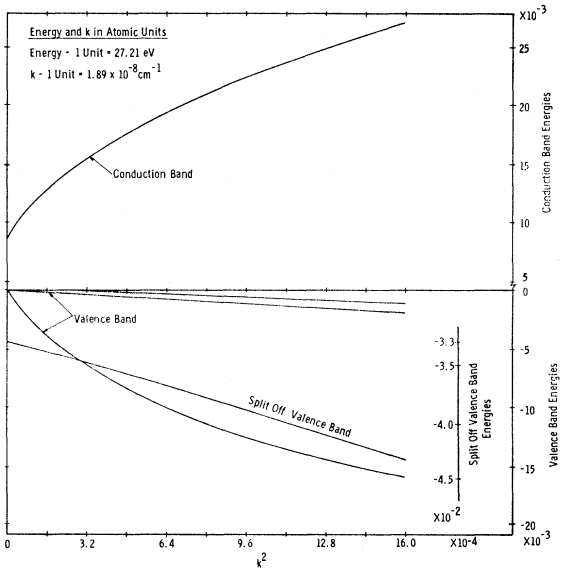

FIG. 5. Energy versus squared wave vector ($\phi=54.7°$, [111] direction).

[14] F. Herman, C. D. Kuglin, K. F. Kuff, and R. L. Kostum, Phys. Rev. Letters **11**, 541 (1963).

[15] H. R. Phillip and H. Ehrenreich, Phys. Rev. **129**, 1550 (1963).

[16] H. Ehrenreich, H. R. Phillip, and J. C. Phillips, Phys. Rev. Letters **8**, 59 (1962).

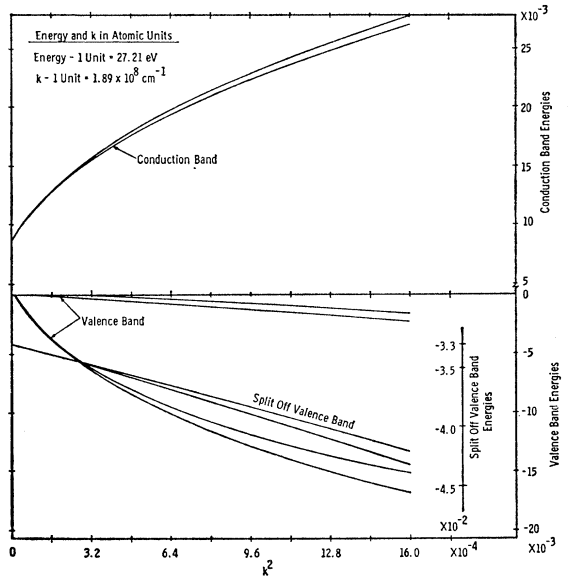

FIG. 6. Energy versus squared wave vector ($\phi=70°$).

taken H_2 to be $\frac{1}{2}H_1$. This leaves the linear-k terms with an influence comparable to that which they exert in Kane's original analysis. The contribution of Γ_5 levels (H_3) is negligible, since the component of potential V which is effective in the spin-orbit matrix element must transform as some representation other than the unit representation Γ_1, in order to give a nonzero contribution. Such components will have comparatively small derivatives. The second-order spin-orbit energies J_3 and J_4 are of the order of 10^{-3} to 10^{-4} a.u., and are neglected.

Finally we may estimate the parameters A and D. The parameter A accounts for $\mathbf{k}\cdot\mathbf{p}$ interactions with Γ_1 bands. The closest Γ_1 (apart from the conduction band) is likely to occur at an energy of the order of 1 Ry above the conduction band, the binding of the lower atomic S states is of the order of 10 Ry. Assuming a squared matrix element of the order of 10 eV and gap of 1 Ry, we have, for a higher Γ_1 level, $A=-0.6\ \hbar^2/2m$. Similar arguments hold for Γ_5 levels, and the coefficient D, which is probably of the order of $D=-0.2\ \hbar^2/2m$. In order to arrive at an estimate of P^2 consistent with experiment, the matrix of Fig. 1 was diagonalized for zero magnetic field using the above values of the parameters and different values of P, for a series of k values sufficient to give an accurate indication of the electron effective mass m_e at the bottom of the conduction band. The value arrived at for $m/m_e=77$: $P^2=0.466$, is fairly close to Kane's original estimate.

IV. BAND STRUCTURE IN ZERO FIELD

Figures 3 through 7 show typical computer plots of the zero-field conduction and valence bands obtained by diagonalizing the matrix of Fig. 1, using the parameters of the previous section. In each case, the k vector is chosen to lie in the (110) plane, containing [100], [111], and [110] directions. ϕ is the angle between the k vector and the ⟨100⟩ axis. In these plots the band edges and energy scales for the conduction and split-off valence bands are arbitrarily displaced by a fixed amount from the energy of the valence-band edge, taken as origin. The band symmetries imposed by the zinc-blende double group[10] are clearly satisfied. The Γ_8 valence band shows the requisite first-order splitting (Fig. 2 of Ref. 10)—the heavy-hole bands cross on the ⟨100⟩ axes, the light holes cross on the ⟨100⟩ and ⟨111⟩ axes. More complete results show that the Γ_6 conduction band and the Γ_7 split-off band follow closely the predicted pattern of third-order splitting (Fig. 4 of Ref. 10). Slight warping of the light-mass bands is evident from the figures: the conduction-band anisotropy at high k values is in agreement with De Haas-Shubnikov measurements on degenerate n-type InSb.[17] The expected pronounced anisotropy of the heavy-hole bands can also be seen. The following heavy-hole masses along the indicated axes are obtained: $m_{100}=0.239m$, $m_{111}=0.490m$, and $m_{110}=0.376m$. These last two are average values for the spin-split bands.

V. THE MAGNETIC-FIELD HAMILTONIAN

In the presence of a magnetic field, the Hamiltonian matrix of Fig. 1 operates on eight different wave functions, each an infinite sum over the (harmonic-oscillator) index n, of terms under the summation sign in (2.2). Pursuing the harmonic oscillator formalism, the transverse components of the wave vector are written in terms of raising and lowering operators a^+ and a^-,

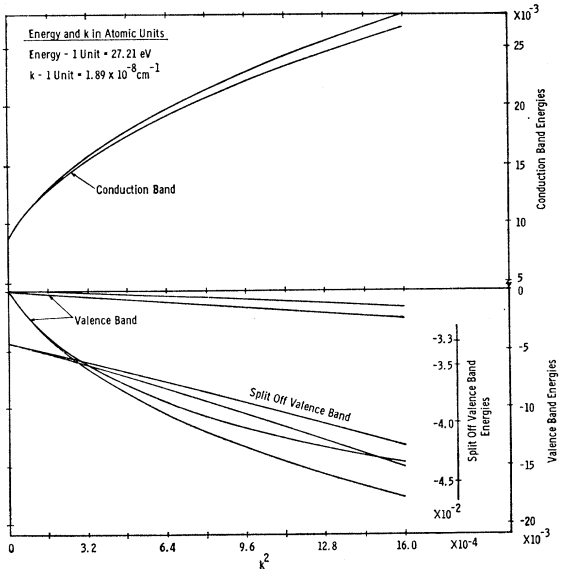

FIG. 7. Energy versus squared wave vector ($\phi=90°$, [011] direction).

[17] G. A. Antcliffe and R. A. Stradling, Phys. Letters **20**, 119 (1966).

$f\left(2a^{+}a+1+d^{2}\right)+1+\epsilon_{o}/s$	0	$iP_1a^{+}-iP_2a$	$-P_2a^{+}-P_1a$	$i\left(a^{2}-a^{+2}\right)\gamma/2-ipd/\sqrt{s}$	0	0	0
0	$f\left(2a^{+}a+1+d^{2}\right)-1+\epsilon_{o}/s$	0	0	0	$iP_1a^{+}-iP_2a$	$-P_2a^{+}-P_1a$	$i\left(a^{2}-a^{+2}\right)\gamma/2-ipd/\sqrt{s}$
$iP_2a^{+}-iP_1a$	0	$\left(2\beta+\alpha'\right)a^{+}a+\frac{\alpha'}{2}\left(a^{+2}+a^{2}\right)+Q_3$	$i\nu\left(a^{2}-a^{+2}\right)/2-iQ_9$	$P_3\left(a^{+}+a\right)$	$\zeta\left(a-a^{+}\right)/\sqrt{2s}$	$iHa\sqrt{2s}$	P_5
$-P_1a^{+}-P_2a$	0	$\frac{i\nu}{2}\left(a^{2}-a^{+2}\right)+iQ_9$	$\left(2\beta+\alpha'\right)a^{+}a-\frac{\alpha'}{2}\left(a^{+2}+a^{2}\right)+Q_4$	$iP_4\left(a^{+}-a\right)$	$iHa\sqrt{2/s}$	$-\zeta\left(a^{+}+a\right)/\sqrt{2s}$	iP_6
$i\left(a^{2}-a^{+2}\right)\gamma/2+ipd/\sqrt{s}$	0	$P_3\left(a^{+}+a\right)$	$iP_4\left(a^{+}-a\right)$	$2\beta a^{+}a+Q_5$	P_6	iP_5	$\zeta a^{+}\sqrt{2/s}$
0	$iP_2a^{+}-iP_1a$	$\zeta\left(a^{+}-a\right)/\sqrt{2s}$	$-iHa^{+}\sqrt{2/s}$	P_6	$\left(2\beta+\alpha'\right)a^{+}a+\frac{\alpha'}{2}\left(a^{+2}+a^{2}\right)+Q_6$	$i\nu\left(a^{2}-a^{+2}\right)/2-iQ_{10}$	$-P_4\left(a^{+}+a\right)$
0	$-P_1a^{+}-P_2a$	$-iHa^{+}\sqrt{2/s}$	$-\zeta\left(a^{+}+a\right)/\sqrt{2s}$	$-iP_5$	$\frac{i\nu}{2}\left(a^{2}-a^{+2}\right)+iQ_{10}$	$\left(2\beta+\alpha'\right)a^{+}a-\frac{\alpha'}{2}\left(a^{+2}+a^{2}\right)+Q_7$	$iP_3\left(a-a^{+}\right)$
0	$i\left(a^{2}-a^{+2}\right)\gamma/2+ipd/\sqrt{s}$	P_5	$-iP_6$	$\zeta a\sqrt{2/s}$	$-P_4\left(a^{+}+a\right)$	$iP_3\left(a-a^{+}\right)$	$2\beta a^{+}a+Q_8$

FIG. 8. Matrix of Fig. 1 in terms of raising and lowering operators.

following Luttinger.[3] For a magnetic field in the z direction,

$$i[k_x,k_y]=eH/\hbar c=s. \tag{5.1}$$

We write

$$k_x=-(a^{+}+a^{-})(\tfrac{1}{2}s)^{1/2},\quad k_y=i(a^{+}-a^{-})(\tfrac{1}{2}s)^{1/2},\quad k_z=d\sqrt{s} \tag{5.2}$$

$$\{k_xk_y\}=-i(a^{+2}-a^{-2})\tfrac{1}{2}s. \tag{5.3}$$

Energies may be normalized to the unit

$$\tfrac{1}{2}\hbar\omega_c=\hbar^2s/2m, \tag{5.4}$$

which is factored out of the Hamiltonian. The remaining 8×8 operator Hamiltonian is shown in Fig. 8. The following substitutions and abbreviations have been made there:

$$(\hbar^2/2m)f=F+\hbar^2/2m,\quad (\hbar^2/2m)\beta=C+D+\hbar^2/2m,$$
$$(\hbar^2/2m)\gamma=2G,\quad (\hbar^2/2m)\alpha=A+B+\hbar^2/2m,$$
$$(\hbar^2/2m)\nu=D_1,\quad \alpha'=\alpha-\beta$$
$$(\hbar^2/2m)\zeta=H_6,\quad (\hbar^2/2m)j=J_7,$$
$$(\hbar^2/2m)p=P,\quad (\hbar^2/2m)\delta=-E_2-J_6,$$
$$(\hbar^2/2m)H=H_7,\quad (\hbar^2/2m)\epsilon_0=E_g,$$
$$(\hbar^2/2m)s=\sigma,\quad (\hbar^2/2m)\mu=C_1,$$

$$P_1=\gamma d/\sqrt{2}+p/(2s)^{1/2},\quad P_2=\gamma d/\sqrt{2}-p/(2s)^{1/2},$$
$$P_3=H/(2s)^{1/2}-\nu d/\sqrt{2},\quad P_4=H/(2s)^{1/2}+\nu d/\sqrt{2},$$
$$P_5=Hd/(s)^{1/2}+j/s,\quad P_6=Hd/(s)^{1/2}-j/s,$$
$$Q_3=\beta+\alpha'/2+\beta d^2+1+\zeta d/(s)^{1/2}-\delta/s,$$
$$Q_4=\beta+\alpha'/2+\beta d^2+1-\zeta d/(s)^{1/2}-\delta/s,$$
$$Q_6=\beta+\alpha'/2+\beta d^2-1-\delta/s-\zeta d/(s)^{1/2},$$
$$Q_7=\beta+\alpha'/2+\beta d^2-1-\delta/s+\zeta d/(s)^{1/2},$$
$$Q_5=\beta+(\alpha'+\beta)d^2+1-\delta/s,$$
$$Q_8=\beta+(\alpha'+\beta)d^2-1-\delta/s,$$
$$Q_9=\mu+j/s,$$
$$Q_{10}=\mu-j/s.$$

We also use

$$Q_1=f(1+d^2)+1+\epsilon_0/s,$$
$$Q_2=f(1+d^2)-1+\epsilon_0/s.$$

As we have said, the matrix of Fig. 8 is intended to operate on wave functions which are expressed as infinite series of harmonic-oscillator functions, to produce for diagonalization a matrix of dimensions ∞ by ∞. The development of this matrix is treated in Appendix II.

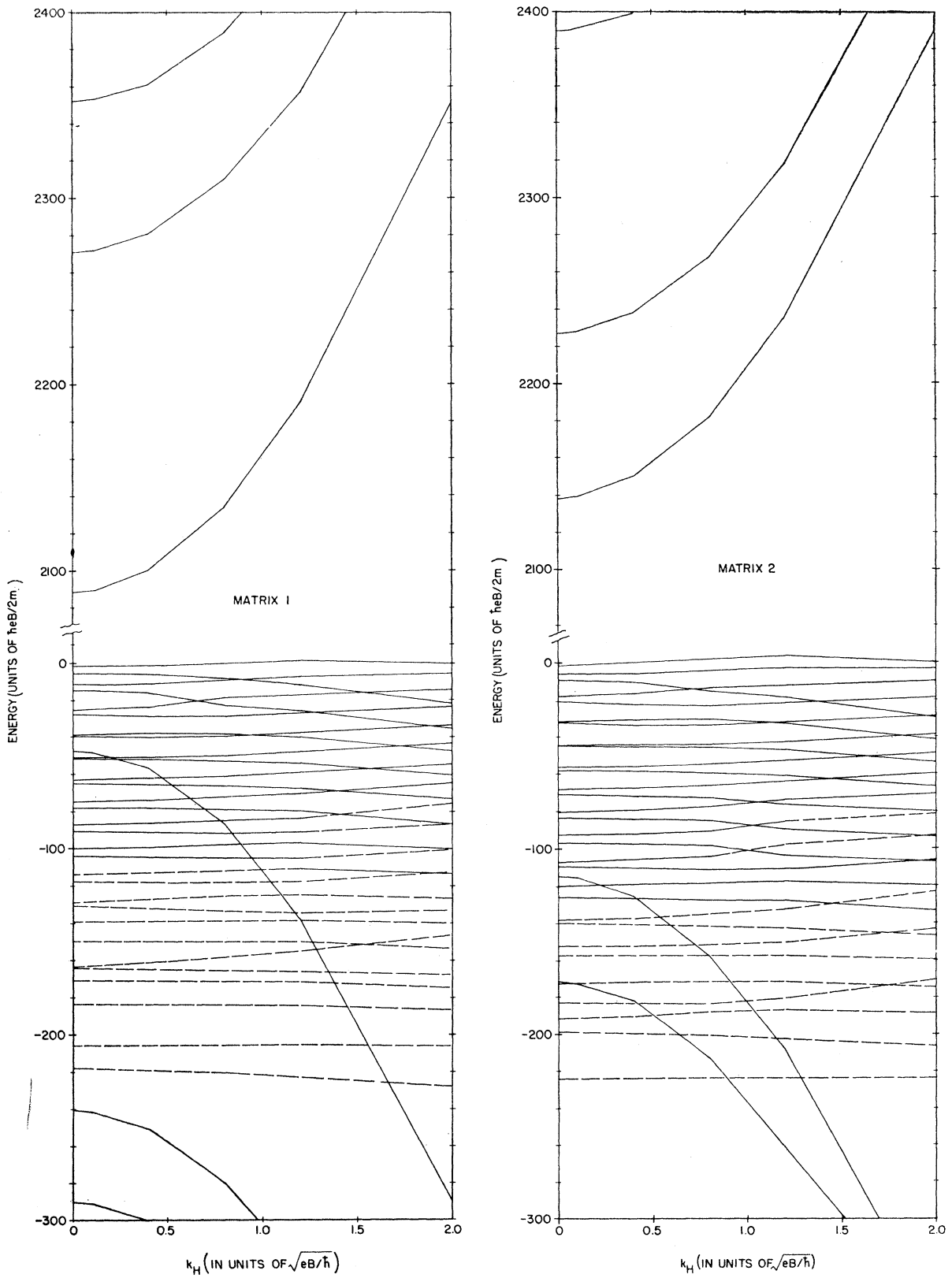

FIG. 9. Landau levels of InSb, $H_{100}=20$ kG: (a) matrix 1, (b) matrix 2.

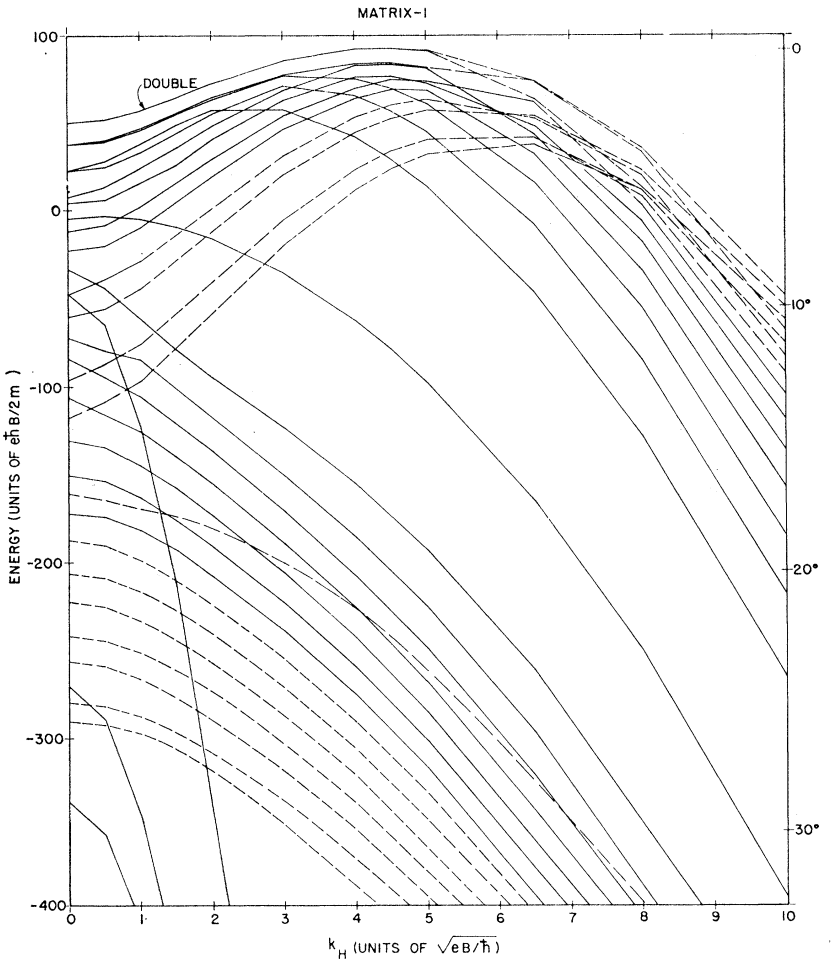

FIG. 10. Valence-band Landau levels of InSb, $H_{100}=1$ kG, matrix 1.

VI. MATRIX ELEMENTS

In the presence of a magnetic field described by the vector potential $\mathbf{A}_0$ of (2.4), the incidence of an electromagnetic signal $\mathbf{A}_1$ produces a perturbation

$$H'=-(e/m)\mathbf{A}_1(\boldsymbol{\pi}-e\mathbf{A}_0), \tag{6.1}$$

where

$$\boldsymbol{\pi}=\mathbf{p}+\hbar\boldsymbol{\sigma}\times\nabla V/4m^2c^2. \tag{6.2}$$

The spin-orbit contribution to $\boldsymbol{\pi}$ can be neglected in good approximation. Writing

$$\begin{aligned}\mathbf{A}_1&=(A^+,A^-,A_z),\\ \mathbf{p}&=(p^+,p^-,p_z),\end{aligned} \tag{6.3}$$

where

$$\begin{aligned}A^\pm&=(A_x\pm iA_y)/\sqrt{2},\\ p^\pm&=(p_x\pm ip_y)/\sqrt{2},\end{aligned} \tag{6.4}$$

and neglecting the spin-orbit term in (6.2),

$$H'=-(e/m)\{A^+p^-+A^-p^+ +A_zp_z +eBy(A^++A^-)/\sqrt{2}\}. \tag{6.5}$$

The diagonalized wave functions are of the form (2.2). Operation of H' on the summand of (2.2) can clearly be broken down into 3 classes: operation on the exponential factor, on the atomic-like band edge functions, and on the envelope functions $f_n(y)$. Operation on the exponential factor generates a diagonal matrix with elements $-(e/m)\hbar\mathbf{k}\cdot\mathbf{A}_1$ representing zero net absorption in the absence of collisions, and this term is ignored. Taken between the band-edge functions, the matrix elements of y may be neglected, and (6.5) may be written in good approximation

$$H'=-(e/m)\{A_zp_z+A^+p^-+A^-p^+\}. \tag{6.6}$$

For operations on the envelope functions, we have for $e<0$

$$\begin{aligned}&\partial/\partial x\equiv 0\equiv\partial/\partial z,\quad s=-eB/\hbar,\\ &\hbar(\partial/\partial y+sy)=(2s)^{1/2}a^-,\\ &\hbar(\partial/\partial y-sy)=-(2s)^{1/2}a^+,\end{aligned}$$

where the raising and lowering operators are defined through

$$\begin{aligned}a^-f_n&=(n)^{1/2}f_{n-1},\\ a^+f_n&=(n+1)^{1/2}f_{n+1}.\end{aligned}$$

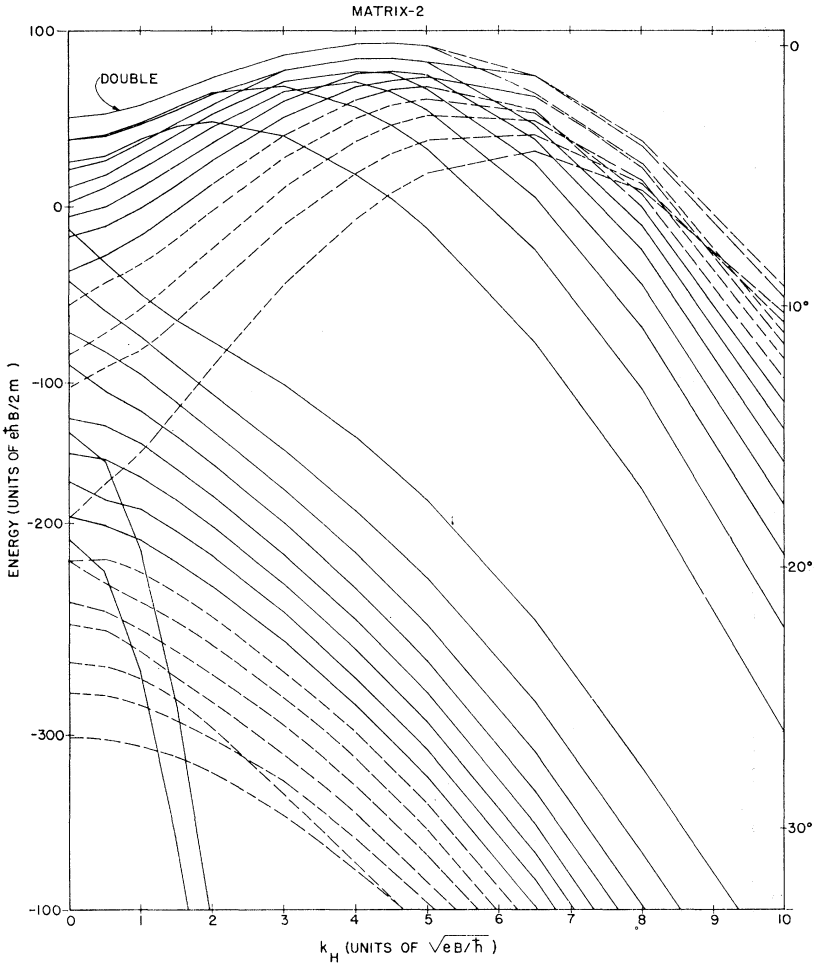

FIG. 11. Valence-band Landau levels of InSb, $H_{100}=1$ kG, matrix 2.

Gathering terms therefore we have finally

$$H'=-(e/m)\{A_z p_z+A^+(p^- -\hbar(s)^{1/2}a^-) +A^-(p^+-\hbar(s)^{1/2}a^+)\}, \quad (6.7)$$

where the p's operate on the band edge functions and the a's on the envelope functions, respectively. As shown in Appendix I, for a simple (Kramers-degenerate) band, the intraband matrix elements of p are proportional to those of a, and the effective-mass approximation is recovered. The matrix elements displayed below are appropriate combinations of $p^{\pm}$, $a^{\pm}$, as they appear in (6.7).

VII. LANDAU LEVELS

Results are presented here for two values of field only; 20 kG, representative of high-field cyclotron resonance at millimeter wavelengths, and of interband magneto-optical experiments, and 1 kG, representative of low-field cyclotron resonance. The full Hamiltonian of the previous sections is truncated to 240×240 and diagonalized for different values of k_z, to yield the diagrams of Figs. 9 through 11. The complete matrix decouples into two separate matrices of 120×120. To minimize confusion, the results of diagonalizing matrix 1 and matrix 2 are shown separately. For the 1 kG results, the conduction bands are omitted from the diagrams since these are of minor interest. Truncation of the matrices at an arbitrary point introduces an unknown error into each level. Fortunately, the nonzero elements of the Hamiltonian matrix occupy a narrow band close to the diagonal, so that the error is small except near the truncation point. The error may be estimated by truncating more severely, say to 80×80, and comparing the results with the 120×120 diagonalization. The results show that the first 60 levels from each 120×120 matrix are quite reliable, and certain of the later levels may be fairly accurate. A test was devised, based on the Levi-Hadamard theorem[18] in the theory of matrices, which gave an upper bound on the error incurred in the truncation procedure. While indicating gratifying accuracy for the conduction-band levels, this test tended to disqualify many of the valence-band

[18] E. Bodewig, *Matrix Calculus* (North-Holland Publishing Company, Amsterdam, 1959), 2nd ed., p. 67.

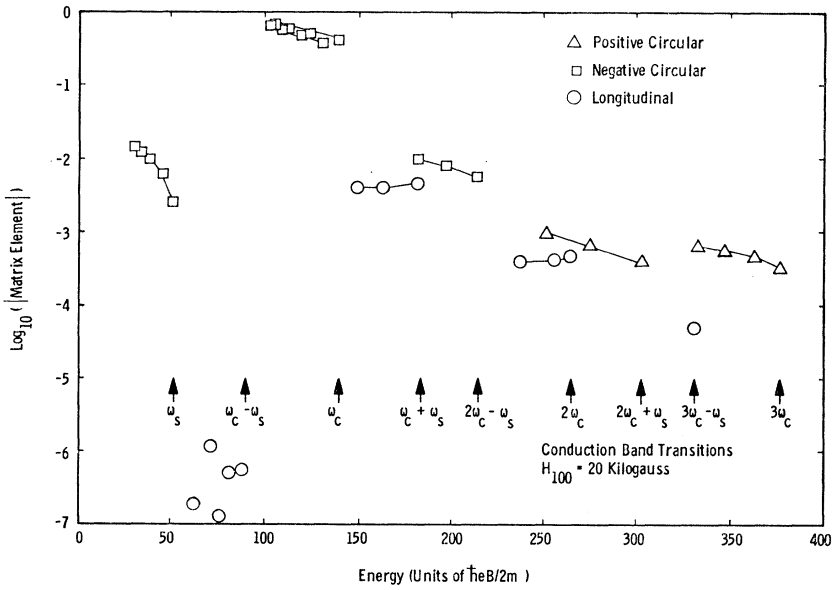

FIG. 12. Intraband absorption matrix elements for the conduction band, $H_{100}=20$ kG, in units of P.

levels validated by the "second truncation" test. Levels of doubtful accuracy are shown dashed in the figures.

To obtain the figures, the energy-level spectrum is calculated for different regularly spaced values of k_z. The computer program causes a print-out of the wave function constitution for each datum point. Straight lines are used to join up points of corresponding wave function, to give an impression of the band structure, without artificial smoothing, however. The coarse spacing of the points in k_z may give a false impression of certain detail, for example, the light-hole bands should clearly meet the central axis at right angles.

Figures 9(a) and 9(b) show band detail near the center of the zone only, for comparison with results of transition-probability computations presented below. Energy-level computations extended in k space well beyond the valence-band maxima show that the heavy-hole bands exhibit the same general behavior at 20 kG as those calculated by Evtuhov[12] for Ge. In particular, the Landau level crossing and the presence of maxima away from $k_H=0$ are observed in both cases, presumably owing to valence-band warping. The effects of the linear-k terms peculiar to the zinc-blende structure are more prominent at low magnetic fields (Figs. 10 and 11).

VIII. CONDUCTION-BAND COMBINATIONAL RESONANCE

The absolute values of the matrix elements for the dominant transitions among the lower levels of the conduction band, at 20 kG, and for positive, negative, and longitudinal polarization of the electromagnetic field, are shown plotted (in units of P) on a logarithmic scale in Fig. 12. Qualitatively similar results are obtained for a 1 kG field. The abscissae of this and all subsequent figures give the g values for the transitions (or alternatively, energy difference in units of $\hbar eB/2m$).

The nonparabolic nature of the band causes a dispersion of the points for a given series along the energy scale, and the "series limits" are indicated by arrows in the figure. Owing to the zinc-blende inversion-asymmetry terms in the Hamiltonian, weakly allowed electric dipole transitions involving spin changes are observed. Electric dipole transitions for negative circular polarization are seen at the spin-resonance energy $\hbar\omega_s$ (cf. the positive circular polarization required for magnetic dipole transitions) at the cyclotron resonance energy $\hbar\omega_c$ and the combinational energy $\hbar(2\omega_c-\omega_s)$. For positive circular polarization, transitions occur at $3\hbar\omega_c$ and at $\hbar(2\omega_c+\omega_s)$, and for longitudinal polarization ($\mathbf{E}\|\mathbf{B}_0$) at $\hbar(\omega_c-\omega_s)$, $\hbar(\omega_c+\omega_s)$, and $2\hbar\omega_c$. Such transitions have been considered in the effective-mass approximation in a series of papers by Rashba

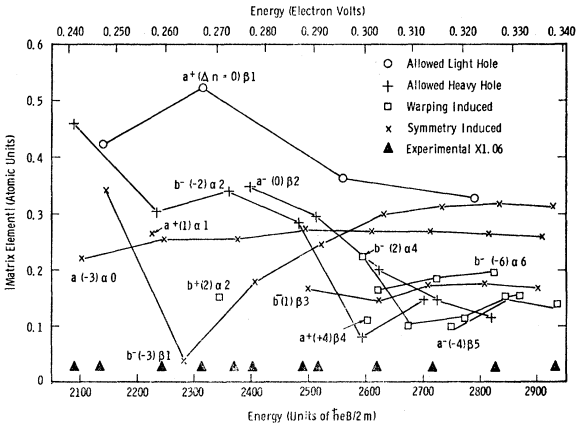

FIG. 13. Interband matrix elements in atomic units—longitudinal polarization.

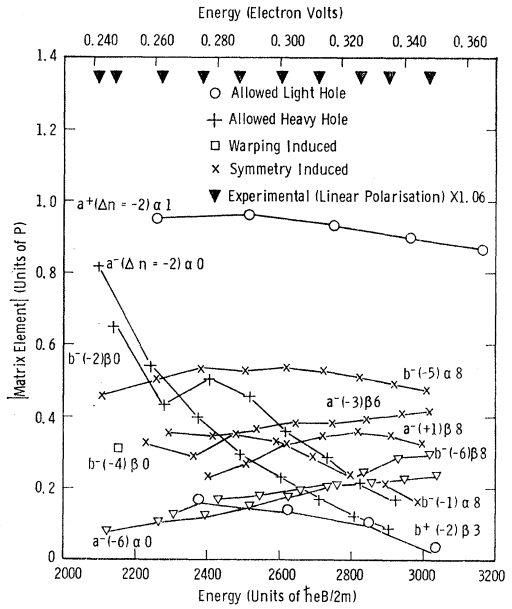

FIG. 14. Interband matrix elements in units of P—positive circular polarization.

and co-workers.[6,7] The [100] magnetic-field direction chosen in this paper selects out the peak of the Ω_{II} function of Rashba and Sheka,[6] all other angular functions being zero for this orientation. The selection rules exhibited by the transitions in Fig. 12 are in accord with the results of Ref. 6. At the same time the square roots of the relative intensities of the lines at ω_s, $\omega_c-\omega_s$, $\omega_c+\omega_s$, $2\omega_c-\omega_s$, and $2\omega_c+\omega_s$ should be in the ratios 0.695:0.0:2.0:2.23:0.89, which are in satisfactory agreement with the "series limit" points in Fig. 12.

By successively setting the coefficient G and the coefficients of the "linear-k" terms in the Hamiltonian equal to zero, it is found that the transitions at ω_s and $2\omega_c-\omega_s$ are caused predominantly by G, those at $2\omega_c$ and $2\omega_c+\omega_s$ by the linear-k terms of the valence band. As might be expected, the cyclotron resonance matrix elements, and those of the $3\omega_c$ transition (see Appendix I) are unaffected.

For a simple parabolic band, the cyclotron resonance matrix elements would increase as $n^{1/2}$ where n is the Landau number of the upper state. Because of the nonparabolicity of the band, the matrix elements at 20 kG rise much more slowly than $n^{1/2}$, reflecting the steady increase of m^* away from the band edge.

IX. INTERBAND TRANSITIONS

Figures 13, 14, and 15 show the magnitudes of some of the computed matrix elements for interband absorption of radiation of parallel, positive-circular, and negative-circular polarization, respectively. Line positions from the experimental results of Pidgeon and Brown[8] are also indicated in the figures. The interpretation is clearest for the parallel case (Fig. 13) and good agreement is observed if the experimental line spacings are uniformly stretched by 6%. The present computation appears to yield an electron mass 6% low, because of an overestimate of the matrix element P. The corrected value of P^2 is 0.436 a.u. The same stretching has also been applied to the transverse-polarization case (Figs. 14 and 15). In comparing the computed with the experimental results it should be noted that the relative densities of states will tend to emphasize heavy-hole transitions over light-hole transitions in the experiment. Because of the light electron mass, the exciton binding energy corrections[19] for the heavy-hole transitions are small, uniform, and probably unobservable. The corrections for the light-hole transitions produce no significant change in the fine structure of the figures (especially in the "quantum levels" where the longitudinal masses are still large—see Fig. 9), and have therefore not been included.

In labelling the interband transitions, it is natural to attempt an interpretation in terms of the well-known nomenclature for Ge.[3,4,8] This meets with the difficulty that the diagonalized energy level scheme for the zinc-blende valence band represents a large perturbation from the corresponding scheme without the inversion asymmetry terms (the "quasi-Ge" model), arising as follows. The valence bands in the quasi-Ge model are closely spaced in energy, with splittings proportional to magnetic field B. The perturbing terms while small are in general still appreciable compared with these splittings. The linear-k terms have matrix elements pro-

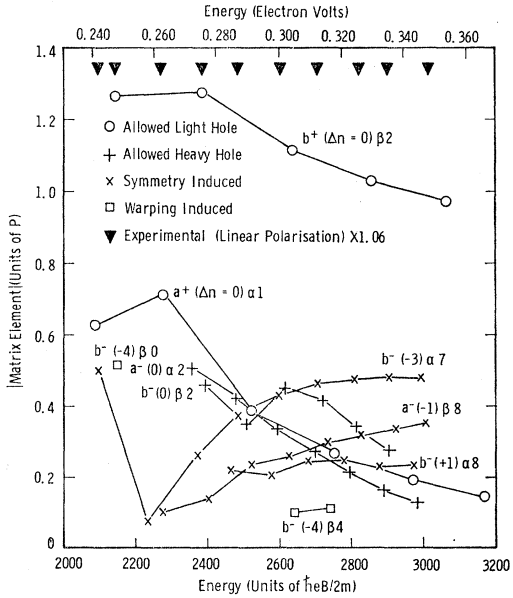

FIG. 15. Interband matrix elements in units of P—negative circular polarization.

[19] R. J. Elliott and R. Loudon, J. Phys. Chem. Solids **15**, 196 (1960).

portional to $B^{1/2}$ and $n^{1/2}$, whereas the matrix element G generates matrix elements in the reduced Hamiltonian proportional to B and n, approximately. These connect nearby eigenstates of the quasi-Ge model and are found to produce splittings and shifts which are of the order or larger than the original splittings, particularly for low fields and/or large n. A low-order perturbation treatment would be valid therefore only close to the band edge *and* at high magnetic fields. In practice, exact diagonalization of the perturbations produces considerable intermixing of the quasi-Ge eigenfunctions, and consequent modifications in oscillator strengths and expected transition schemes. Simultaneously, the mixing introduces some ambiguity into the parentage of the final levels, and labeling in terms of the parent scheme is no longer unique. In the present instance we have used a correspondence which comes close to minimizing the number of "forbidden" $\Delta n=\pm(1,3,5)$ interband transitions while preserving the energy ordering in the heavy- and light-hole ladders. Some violence is done, however, to the wave function envelope index n, which no longer bears a useful relation to the harmonic-oscillator composition of the final wave function.

In the present problem, diagonalization of the separate matrices 1 and 2 generates two independent sets of levels. Selection rules for electric dipole transitions are that "transverse" polarizations generate transitions from set 1 to set 2, whereas "parallel" polarizations generate transitions which occur within sets 1 and 2 separately. In Luttinger's (Ge) nomenclature, set 1 contains $\alpha 0$, $\alpha 2$, $\alpha 4$, etc., and $\beta 1$, $\beta 3$, $\beta 5$, etc., as well as $b0$, $b2$, $b4$, etc., and $a1$, $a3$, $a5$, etc.; set 2 is complementary to the above. The selection rules are then that for transverse polarization, the interband transitions $b^{\pm}\alpha$ and $a^{\pm}\beta$ have $\Delta n=\pm(1,3,5,\text{etc.})$ and $b^{\pm}\beta$ and $a^{\pm}\alpha$ have $\Delta n=\pm(0,2,4,6,\text{etc.})$. For parallel polarizations,

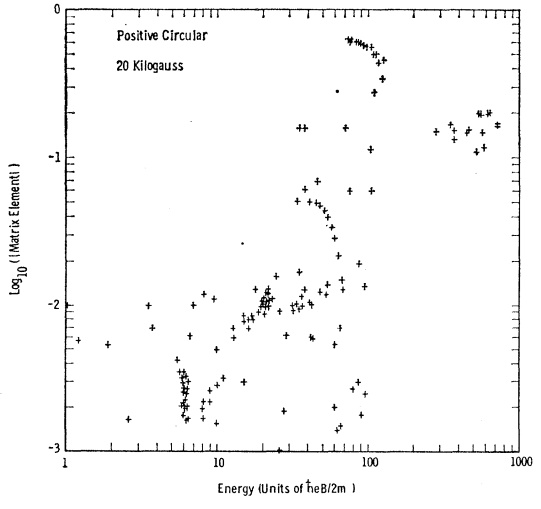

FIG. 16. Valence-band absorption matrix elements—positive circular polarization, 20 kG, units of P.

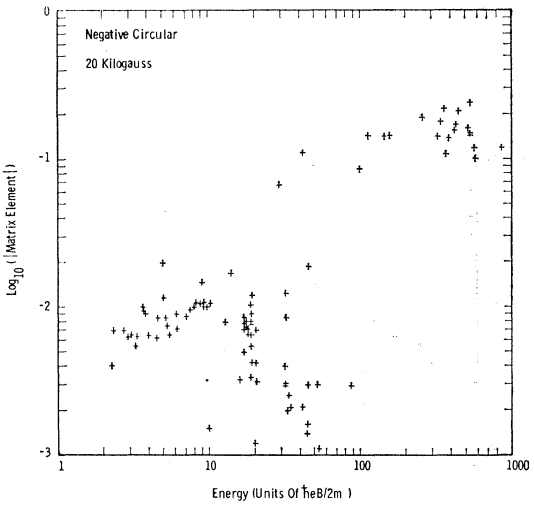

FIG. 17. Valence-band absorption matrix elements—negative circular polarization, 20 kG, units of P.

$a^{\pm}\alpha$ and $b^{\pm}\beta$ have $\Delta n=\pm(1,3,5,\text{etc.})$ and $b^{\pm}\alpha$, $a^{\pm}\beta$ have $\Delta n=\pm(0,2,4,6,\text{etc.})$. These rules include the Ge-like allowed transitions, the "warping induced" transitions, and also "Ge-forbidden" transitions $\Delta n=\pm(1,3,5,\text{etc.})$ due to the center of inversion asymmetry, which we have labelled "symmetry-induced" in the figures.

The above correlation of the present computation with experimental results of Pidgeon and Brown[8] suggests a conduction-band edge "interband" effective mass of $m_e=0.0139m$ and a corresponding "interband" light-hole mass of $0.0152m$ (cf. the hole mass of $0.0159m$ obtainable via the electron mass from Kane's simplified treatment[9]). By comparison, intraband measurements[20] yield a band-edge value of $0.0145m$ at 77°K. Owing to a region of negative thermal expansion at low temperatures,[21] the dilational contribution to the change in bandgap[22] between 4 and 77°K will be small. Similarly, the calculated polaron correction[23] for the intraband electron mass is also small—of the order of 0.5%. An apparent discrepancy of the order of 4% remains between inter- and intraband measurements of the electron mass, due possibly to strain and/or anisotropy effects.

X. VALENCE-BAND CYCLOTRON RESONANCE

Logarithmic plots of matrix elements for absorption of positive and negative circular polarization in valence band transitions are shown (in units of P) in Figs. 16 and 17, respectively, for a field of 20 kG in

[20] E. D. Palik, G. S. Picus, S. Teitler, and R. F. Wallis, Phys. Rev. **122**, 475 (1961).
[21] S. Novikova, Fiz. Tverd. Tela **2**, 2341 (1960) [English transl.: Soviet Phys.—Solid State **2**, 2087 (1961)].
[22] S. D. Smith, C. R. Pidgeon, and V. Prosser, in *Proceedings of the International Conference on the Physics of Semiconductors, Exeter, 1962* (The Institute of Physics and The Physical Society, London, 1962), p. 301.
[23] T. D. Lee, F. E. Low, and D. Pines, Phys. Rev. **90**, 297 (1953),

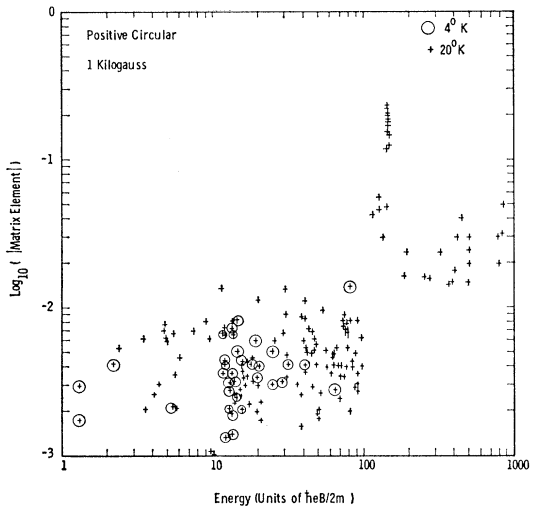

FIG. 18. Valence-band absorption matrix elements—positive circular polarization, 1 kG, units of P.

the [100] direction. The large field is not inappropriate for heavy-hole cyclotron resonance at millimeter wavelengths. Plots for a 1-kG field (Figs. 18 and 19) are shown for the $k_z=0$ region. Although this does not qualify as a "band edge" position, densities of states will generally be highest at this point, so that this will be the region observed experimentally. An impression of the expected cyclotron resonance spectrum may be gained by imagining a base line sloping upwards from left to right at about 45° in the figures. This takes roughly into account the varying energy denominator and densities of states which enter into the transition probability. The spectrum may then be estimated by integrating the density of points by eye, relative to this base line.

Figures 18 and 19 display transitions (circles) which involve states close to the top of the valence band, and which might be observed therefore at helium temperatures. Structure which would be interpreted in cyclotron resonance as a positive mass hole resonance would be expected at $m^*=0.15m$ and a negative mass hole at $m^*=0.14m$, with isolated lines at higher mass numbers up to $1.6m$. These results may be compared with experiments reported by Dresselhaus, Kip, Kittel, and Wagoner,[24] in particular a hole mass of $0.18m$ at 1550 G (24 kMc/sec). The strong band of light-hole transitions at $m^*=0.0143m$ will not be observed at helium temperatures in lightly doped p-type material since, as is clear from Fig. 10, the light holes will be frozen out at temperatures below 10°K. This is in fact observed[25] in the disappearance of the light-hole signal in this region. This possibility provides a direct experimental method of estimating the magnitude of the linear-k coefficients, since these enter to determine the energy difference between the edge of the valence band and the lowest light-hole level. On applying the 6% correction factor of the previous section, the band edge light-hole mass at low field is found to be $0.0152m$. This may be compared with cyclotron resonance measurements of Bagguley *et al.*[5] and a more recent measurement of Stradling,[26] yielding light-hole masses of $0.021\pm0.005m$ at 20°K and $0.0202\pm0.0015m$ at 77°K, respectively. Allowing for nonparabolic effects, the latter value indicates a band-edge light-hole mass in the region of $0.017m$. Again the applicable band gap and polaron corrections are negligible, and the difference may be attributed to parameter uncertainties and the considerable experimental difficulties. Figures 18 and 19 show that as the temperature is raised (crosses) the heavy-mass cyclotron resonance spectrum at low fields will become a broad featureless band of absorption, apparently covering the mass range from 0.06 to $1.6m$.

In Fig. 16 the light-hole line is shown dispersed by the nonparabolicity of the band, having a series-limit mass of $0.016m$ in agreement with the results of Pidgeon and Brown.[8] However, application of the correction to P discussed above would raise this to $0.017m$, in better agreement with cyclotron-resonance results. A similar series of transitions is seen for the light-hole spin resonance, having a limit in the region of $g=70$. In these plots, the relevant energy levels are taken deep into the bands, so that they represent a fairly high experimental temperature, of the order of 100°K. Figure 16 shows that positive mass hole resonances are expected in the neighborhood of $m^*=0.095m$ and $m^*=-0.4m$, respectively. Other isolated lines may be observed at relatively high mass numbers. These results can be compared with experimental heavy-hole masses[5,8] of $0.34\pm0.03m$ and $0.32m$ for the [100] direction. It is clear from the figures that the dispersion of the lines

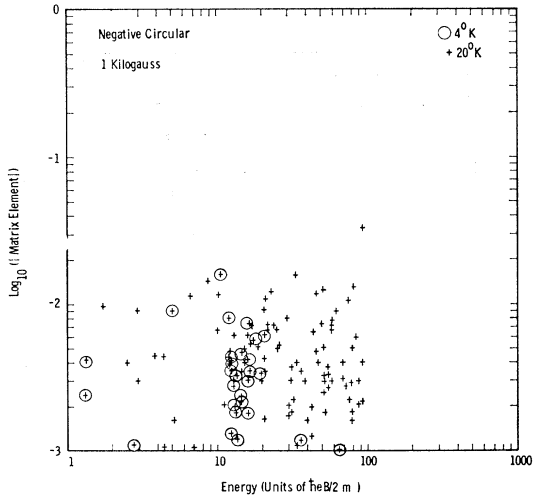

FIG. 19. Valence-band absorption matrix elements—negative circular polarization, 1 kG, units of P.

[24] G. Dresselhaus, A. F. Kip, C. Kittel, and G. Wagoner, Phys. Rev. **98**, 556 (1955).

[25] M. L. A. Robinson (private communication).

[26] R. A. Stradling (private communication).

and the variation of the spectrum with variation in temperature will give rise to complex behavior which could, if interpreted in terms of a few isolated lines broadened by collisions, lead to erroneous conclusions on line-broadening mechanisms and their relative strengths. The polaron effective-mass correction is of the order of 0.5% for electrons and light holes, 2.5% for mass 0.32, and 4.4% for mass 1.0.

XI. CONCLUSIONS

Sample machine calculations of Landau levels in InSb for one magnetic-field direction have demonstrated the complexity of the valence band level structure,[10] and accounted approximately for the diverse experimental results[5,8,24] on heavy-hole masses. The calculated matrix elements for interband and intra-conduction-band transitions in the model used are in satisfactory agreement with other experimental and theoretical results[4,8,7] where these overlap. Comparison with the experimental interband spectra[8] gives for band edge electron and light-hole masses $m_e^*=0.0139m$ and $m_{\text{l.h.}}^*=0.0152m$, respectively. The corresponding value of the parameter P^2 is 0.436 a.u., assuming an energy gap of 0.2355 eV.

ACKNOWLEDGMENTS

The authors are grateful to R. A. Stradling, C. R. Pidgeon, and M. L. A. Robinson for communication of their results prior to publication, and for helpful correspondence.

APPENDIX I

One result of the above analysis is that the matrix elements for intraband transitions between Landau levels are due mainly to "optical" transitions, with the selection rules $\Delta n=\pm1$, ±3, etc. Here we employ the Luttinger-Kohn analysis to justify this to order k^2.

The velocity operator associated with the Schrödinger equation including spin-orbit coupling is

$$\pi/m=\mathbf{p}/m+\hbar\sigma\times\nabla V/4m^3c^2, \tag{A1}$$

and the time-dependent perturbation operator for small steady applied magnetic fields is approximately $-\pi e\mathbf{A}_1/m$. We expand the initial and final states of the magnetic field problem in terms of Bloch functions $|lk\rangle=u_{lk}(r)e^{ikr}$, for example,

$$|\Psi^F\rangle=\sum_{lk}|lk\rangle\langle kl|\rangle. \tag{A2}$$

The Bloch functions have their own expansions in terms of L-K band-edge functions, the transformation arising principally through the $\mathbf{k}\cdot\pi$ perturbation. To first order,

$$|lk\rangle=\left\{|l0\rangle+\frac{\hbar\mathbf{k}}{m}\sum_q\frac{|q0\rangle\langle0q|\pi|l0\rangle}{E_l-E_q}\right\}e^{ikr}. \tag{A3}$$

The expansion for $\langle\Psi^I|\pi|\Psi^F\rangle$ breaks into three main terms. The first is

$$\sum_{lkl'k'}\langle|l'k'\rangle\langle u_{l'k'}|u_{lk}\rangle\langle e^{-ik'r}|\pi|e^{ikr}\rangle\langle kl|\rangle, \tag{A4}$$

which is approximately

$$\pi_1=\sum_{lkl'k'}\langle|l'k\rangle\hbar k\delta_{kk'}\delta_{ll'}\langle kl|\rangle=\hbar k. \tag{A5}$$

The second term is

$$\begin{aligned}\pi_2&=\sum_{lkl'k'}\delta_{kk'}\langle|l'k'\rangle\langle0l'|\pi|l0\rangle\langle kl|\rangle\\&=\sum_{ll'}\langle0l'|\pi|l0\rangle\sum_k\langle|l'k\rangle\langle kl|\rangle.\end{aligned} \tag{A6}$$

The eigenstates of the spin-orbit coupled problem can be chosen so that the application of a magnetic field causes no intermixing of band-edge functions to first order. In this case the expansion (A2) contains only one important l value. If we consider intraband transitions therefore, π_2 is zero, since $\pi_{ll}=0$. The third term is

$$\pi_3=\sum_{lkl'k'}\delta_{kk'}\langle|l'k\rangle\frac{\hbar}{m}\left[\sum_q\frac{\langle0l'|\pi|q0\rangle\langle0q|\mathbf{k}\cdot\pi|l0\rangle}{E_l-E_q}+\frac{\langle0l'|\pi\cdot\mathbf{k}|q0\rangle\langle0q|\pi|l0\rangle}{E_{l'}-E_q}\right]\langle lk|\rangle. \tag{A7}$$

For intraband transitions, the only term of significance in (A7) is that for $l=l'$. From the L-K sum rules,

$$-\frac{2}{m}\sum_q\frac{\pi_{lq}{}^\alpha\pi_{ql}{}^\beta}{E_l-E_q}=\delta_{\alpha\beta}-m\frac{\partial^2\epsilon_l(k)}{\partial k_\alpha\partial k_\beta}. \tag{A8}$$

Finally, therefore,

$$\langle\Psi^I|\pi^\alpha|\Psi^F\rangle=\hbar k^\beta m\partial^2\epsilon_l(k)/\partial k_\alpha\partial k_\beta. \tag{A9}$$

For an isotropic band,

$$\pi_{IF}=\hbar k_{IF}(m/m^*). \tag{A10}$$

In more general terms, the $\mathbf{k}\cdot\pi$ perturbation acting between band edges of opposite parity is responsible for light effective masses in solids. In the effective-mass approximation, a given Landau level of say the conduction band in InSb will consist mainly of s-type atomic functions modulated by some harmonic-oscillator envelope function of order n. The $\mathbf{k}\cdot\pi$ perturbation will admix an appreciable amount of p-type character from the valence bands. In order to preserve the original parity of the original level, these admixtures of opposite-parity atomic functions will be modulated with envelope functions of parity (defined by their order) $n\pm1$, $n\pm3$, $n\pm5$, etc. A given Landau level in a light-effective-mass band therefore will consist of mixtures of opposite-parity atomic functions modulated by opposite-parity envelope functions. As shown above, the principal mechansim (by a factor m/m^*-1) for intraband transitions in such a case are "optical" transitions between the atomic functions. The selection rules for electric dipole transitions between Landau levels will therefore clearly be $\Delta n=\pm1$, ±3, ±5, etc.

APPENDIX II

Here we give a prescription for the generation of an approximate ∞ by ∞ matrix from the operator matrix of Fig. 8. This is developed by operating with the finite matrix on envelope functions whose order lies in the neighborhood of a general function of order n, and generating the infinite matrix by specializing this in turn to the cases $n=0$, $n=1,\cdots\infty$. The presence in the operator matrix of Fig. 8 of terms in a^2, a, a^0, a^+, and a^{+2} involves envelope functions of order $n-2$, $n-1$, n, $n+1$, and $n+2$. Thus the generating matrix becomes 40×8 rather than 8×8. Instead of writing this out in full, we give an alternative prescription for generating the same infinite matrix using fewer terms than the original derivation, taking advantage of the fact that the final matrix is Hermitian. First construct an $8\times\infty$ matrix consisting of all zeros and add in the following elements:

$$(1,1)=2nf+Q_1,$$
$$(1,5)=-ipd/(s)^{1/2}=(2,8),$$
$$(1,11)=iP_2(n+1)^{1/2}=(2,14),$$
$$(1,12)=P_1(n+1)^{1/2}=(2,15),$$
$$(1,21)=\tfrac{1}{2}i\gamma((n+1)(n+2))^{1/2}=(2,24)=(5,17)=(8,18),$$
$$(2,2)=2nf+Q_2,$$
$$(3,3)=n(2\beta+\alpha')+Q_3,$$
$$(3,4)=-iQ_9,$$
$$(3,8)=P_5,$$
$$(3,9)=iP_1(n+1)^{1/2}=-(6,10),$$
$$(3,13)=P_3(n+1)^{1/2}=(5,11),$$
$$(3,14)=\zeta((n+1)/2s)^{1/2}=-(4,15)=(6,11)=-(7,12),$$
$$(3,15)=iH(2(n+1)/s)^{1/2}=(4,14),$$
$$(3,19)=\tfrac{1}{2}\alpha'((n+1)(n+2))^{1/2}=-(4,20)=(6,22)=-(7,23),$$
$$(3,20)=\tfrac{1}{2}i\nu((n+1)(n+2))^{1/2}=(4,19)=(6,23)=(7,22),$$
$$(4,4)=n(2\beta+\alpha')+Q_4,$$
$$(4,8)=iP_6,$$
$$(4,9)=-P_2(n+1)^{1/2}=(7,10),$$
$$(4,13)=-iP_4(n+1)^{1/2}=(5,12),$$
$$(5,5)=2n\beta+Q_5,$$
$$(5,6)=P_6,$$
$$(5,7)=iP_5,$$
$$(6,6)=n(2\beta+\alpha')+Q_6,$$
$$(6,7)=-iQ_{10},$$
$$(6,16)=-P_4(n+1)^{1/2}=(8,14),$$
$$(7,7)=n(2\beta+\alpha')+Q_7,$$
$$(7,16)=iP_3(n+1)^{1/2}=(8,15),$$
$$(8,8)=2n\beta+Q_8,$$
$$(8,13)=\zeta(2(n+1)/s)^{1/2}.$$

This matrix, with $n=0$, fills the first eight rows of the infinite matrix, the corresponding block, moved eight positions parallel to the diagonal, is occupied by the above with $n=1$, and so on. The lower diagonal half of the matrix is filled by taking the Hermitian conjugate of the triangular matrix generated.

Inspection of the final form shows that it can be rendered real by considering the basis to consist of purely real and purely imaginary wave functions, instead of being all real, as implied by the foregoing. The scheme is as follows. The basis falls naturally into groups of eight. In the odd groups of eight, the second, fourth, fifth, and sixth members are multiplied by $(-i)$. In the even groups, the first, third, seventh, and eighth are multiplied by $(-i)$. This corresponds to a unitary transformation by a diagonal matrix in which the diagonal terms are, respectively, $1, -i, 1, -i, -i, -i, 1, 1$; $-i, 1, -i, 1, 1, 1, -i, -i$; and so on. Examination of the resulting matrix reveals that it can be considered as two decoupled matrices (as in Evtuhov's work[12]). The first of these consists only of elements coming from rows and columns 1, 5, 6, 7; 10, 11, 12, 16, etc., from the original matrix. Similarly, the second matrix can be generated by choosing only elements from rows and columns 2, 3, 4, 8; 9, 13, 14, 15, etc. This allows the diagonalization of twice as large a matrix on a given machine as would be feasible without decoupling.